Pion elastic and inelastic scattering from ^{24}Mg and ^{26}Mg

G. S. Blanpied, J. Hernandez,* C. S. Mishra,† W. K. Mize, and C. S. Whisnant
University of South Carolina, Columbia, South Carolina 29208

B. G. Ritchie
Arizona State University, Tempe, Arizona 85287

C. L. Morris and S. J. Seestrom-Morris
Los Alamos National Laboratory, Los Alamos, New Mexico 87545

C. Fred Moore and P. A. Seidl‡
University of Texas, Austin, Texas 78712

R. A. Lindgren
University of Virginia, Charlottesville, Virginia 22901

B. H. Wildenthal
University of New Mexico, Albuquerque, New Mexico 87131

R. Gilman§
University of Pennsylvania, Philadelphia, Pennsylvania 19104
(Received 18 November 1988; revised manuscript received 6 December 1989)

Reported are measurements of angular distributions of resonance-energy positive and negative pions exciting approximately 40 states in ^{24}Mg and ^{26}Mg. These include the (ground state, 0^+), (1.36 MeV, 2^+), (4.14, 2^+), (5.93, 4^+), (6.44, 0^+), (7.34), (7.55, 3^-), (8.33, 3^-), (9.32, 4^+), (9.97, 5^-), (11.08, 3^-), (12.06), (13.26), (13.96, 3^-), (15.1, $T=1$, 6^-), and (15.4) states in ^{24}Mg and the (ground state, 0^+), (1.81, 2^+), (2.92, 2^+), (3.59, 0^+), (4.31, $2^+ + 4^+$), (4.90, 4^+), (5.31, 2^+), (5.44, 4^+), (5.69, 4^+), (6.86, 3^-), (7.33, 3^-), (7.79, 3^-), (8.17, 3^-), (9.2, possible 6^-), (10.30, 4^+), and (18.1, $T=2$, 6^-) states in ^{26}Mg. The distorted-wave impulse approximation with a Kisslinger form for the optical potential using a π-nucleon t matrix at a shifted energy of -25 MeV was found to explain the elastic scattering data from ^{24,26}Mg in the energy range 116–292 MeV that is spanned by these data. Inelastic distorted-wave impulse approximation calculations employing collective-model deformation parameters were simultaneously fitted to the π^+ and π^- data for each state. The deformation parameters and matrix elements in most cases compare favorably with results from other studies. Published s-d shell-model calculations using one value for the effective charges were found to reproduce the trend of both the strengths and ratios of neutron-to-proton matrix elements for the 2^+ and 4^+ states. The data at the first maximum in the inelastic angular distributions for ^{24}Mg and that from other studies for ^{12}C, ^{28}Si, and ^{40}Ca show that the cross section for π^+ scattering is equal to that for π^- scattering, which forces the proton deformation parameters to be greater than the neutron deformation parameters and gives a ratio of neutron-to-proton elements to be less than unity. This difference from unity is interpreted as a measure of the failure of the model and a systematic error of 11% is assumed to dominate the errors in the results for ^{26}Mg. Coupled-channels calculations employing monopole form factors are compared to data for low-lying 0^+ states in ^{24}Mg and ^{26}Mg.

I. INTRODUCTION

The pion has long been considered a promising probe for distinguishing neutron and proton components of nuclear transition densities. When the experimental resolution was worse than 500 keV, most studies were restricted to elastic scattering and a few inelastic peaks or to p-shell nuclei where the resolution is in many cases less critical. One study that changed this was that reported by K. G. Boyer *et al.*[1] in which calcium isotopes were studied at three energies around the (3,3) resonance: 116, 180, and 292 MeV. The resolution was 300 keV and many inelastic angular distributions were measured. Reported here are similar measurements on isotopes of magnesium in the same energy interval. The good energy resolution, as well as emphasis on obtaining good statistics at a few angles, results in angular distributions for approximately 40 peaks in the two isotopes ^{24}Mg and ^{26}Mg. Results are compared to the few resolvable peaks obtained in previous measurements on both ^{24}Mg and ^{26}Mg.[2–5] The

abundant angular distributions obtained here are also exploited for their spectroscopic value. The results are compared with those obtained from electromagnetic measurements,[6-9] recent 0.8-GeV proton inelastic scattering measurements,[10,11] and shell-model predictions.[12]

II. EXPERIMENTAL DETAILS

Data were obtained using the Energetic Pion Channel and Spectrometer (EPICS) facility at the Clinton P. Anderson Meson Physics Facility (LAMPF) of the Los Alamos National Laboratory. The experimental system, described elsewhere,[13,14] consists of a momentum-dispersing channel and a high-resolution spectrometer. Data were acquired with π^+ and π^- beams incident upon ^{26}Mg at 116, 180, and 292 MeV during one data acquisition period and on a split target of ^{24}Mg and ^{26}Mg at 150 and 180 MeV during another period. The targets consisted of 97 mg/cm^2 ^{24}Mg foils and 200 mg/cm^2 ^{26}Mg foils enriched to greater than 99%. The good projection of the vertical target position for each event allowed the use of strip targets of ^{24}Mg and ^{26}Mg, each covering about one-half of the incident beam spot (8 cm horizontal by 20 cm vertical). In order to obtain good statistics for several excited states, data were acquired only at a few angles, chosen in steps of momentum transfer $L \sim qR$, where $R \sim 3$ fm. During the first run, data were obtained at scattering angles corresponding to $qR \sim 2$, 3, 4 and 6 at 116 and 292 MeV and $qR \sim 2$–8 at 180 MeV. Inelastic spectra up to an excitation of more than 20 MeV were acquired with a resolution of better than 250 keV for most angles. During the second run, data were obtained at $qR \sim 4$ and 6 at 180 MeV and $qR \sim 2$–6 at 150 MeV with resolution at about 330 (250) keV for runs with (without) a proton absorber in the channel.

The cross sections have been determined relative to $\pi^{\pm}+p$ elastic scattering measured at one angle for each energy and compared to phase shifts.[15] CH_2 targets of 152 (74) mg/cm^2 were used in the first (second) beam period. All of the $\pi+p$ runs were performed at an angle where the kinematic separation between $\pi+p$ and $\pi+^{12}$C is 30 MeV, well away from large discrete excitations in ^{12}C. (These angles were 80°, 60°, 55°, and 40° at 116, 150, 180, and 292 MeV, respectively.) The relative normalization between π^+ and π^- cross sections obtained here is determined to be better than ±3% and the absolute normalization is known to ±10%. The relative focal-plane acceptance was measured using elastic scattering at the first maximum in the angular distribution at 180 MeV. Representative spectra corrected for the spectrometer acceptance and normalized as discussed above are given in Figs. 1–3. These spectra are chosen at different values of $L \sim qR$ and illustrate the quality of the

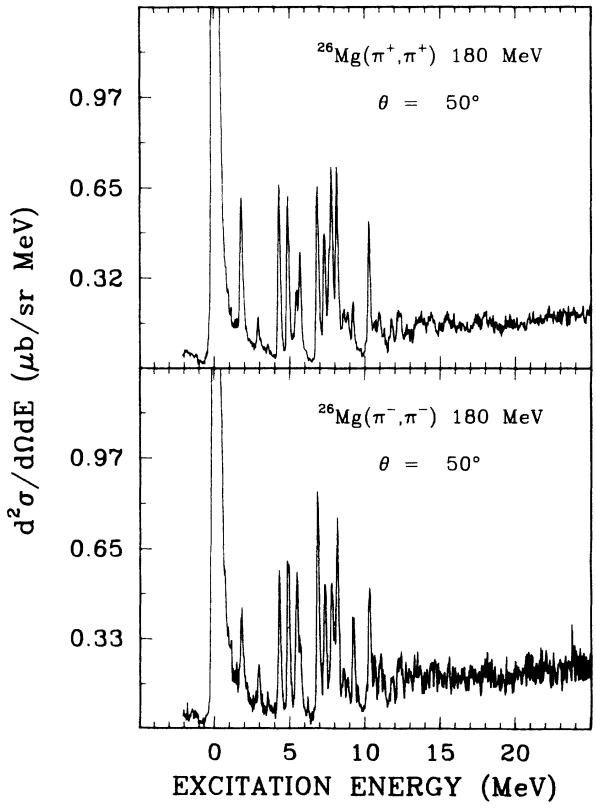

FIG. 1. Spectra of 180 MeV π^+ and π^- inelastic scattering from ^{26}Mg at $\Theta_{lab}=50°$, which corresponds to the first maximum in the angular distributions of pions exciting 4^+ states. The spectra are corrected for the momentum acceptance of EPICS.

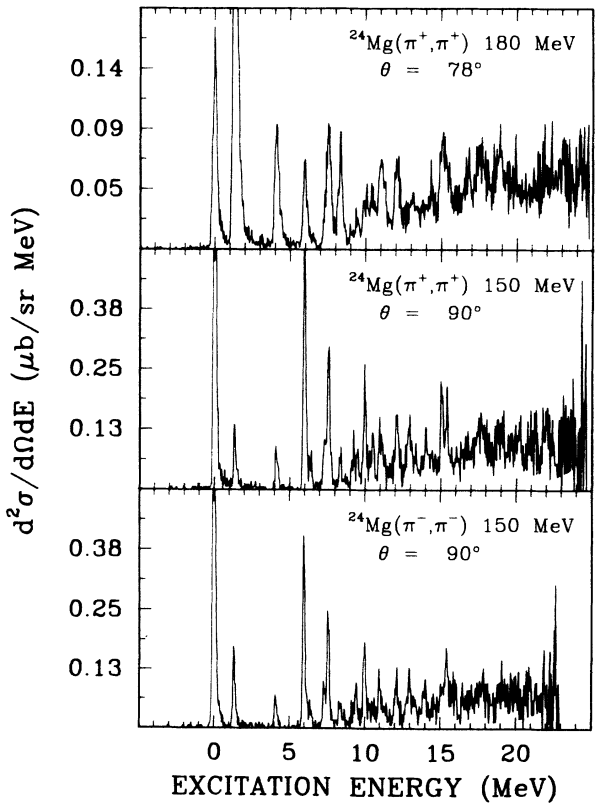

FIG. 2. Spectra of 150 and 180 MeV π^+ and π^- inelastic scattering from ^{24}Mg at angles corresponding to the first maximum for $l=6$ transfer. The (15.1, 6^-, $T=1$) state is evident.

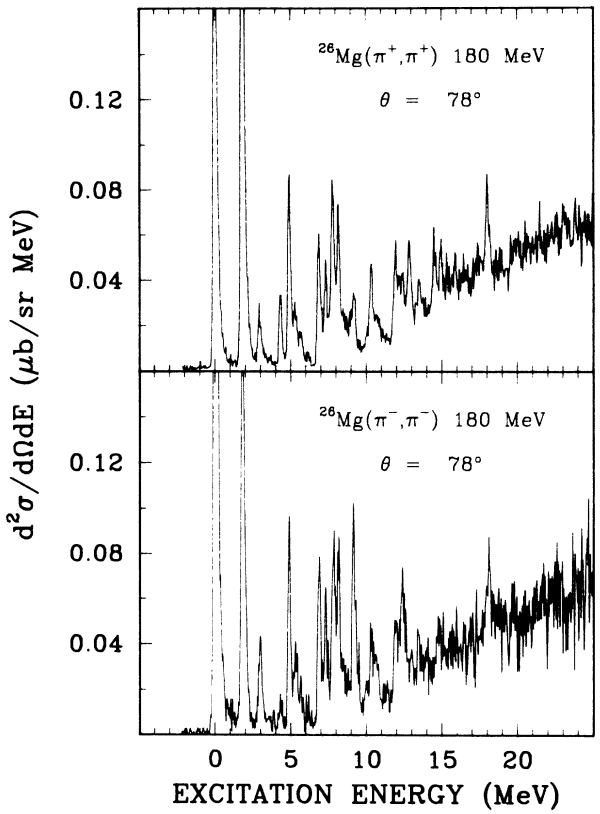

FIG. 3. Spectra of 180 MeV π^+ and π^- inelastic scattering from ^{26}Mg at $\Theta_{lab}=78°$, which corresponds to the first maximum for $l=6$ transfer. The (18.0, 6^-, $T=2$) state is evident.

angular distributions for individual states. Figure 1 illustrates the number and good separation of the peaks at an angle which corresponds to a maximum for $L=4$ angular distributions. In Figs. 2 and 3 one can see peaks corresponding to the excitation of 6^- states in ^{24}Mg and ^{26}Mg.

Areas of peaks were extracted from the spectra using the interactive line-shape fitting program LOAF.[16] Known states in ^{24}Mg, ^{26}Mg, and ^{12}C confirmed the accuracy of the energy calibration. Angular distributions for elastic and inelastic scattering are given in Figs. 4–19. A complete tabulation of the numerical data is on deposit in PAPS.[18] Data for peaks at 10.41, 12.06, 12.88, 13.26, 14.36, 15.1 (6^-), and 15.4 MeV in ^{24}Mg and 6.13, 9.2, 10.97, 11.90, 13.49, 14.49, and 18.0 (6^-) MeV in ^{26}Mg are included in the tabulations but are not shown in the figures.

III. ANALYSES

A. Elastic scattering and low-lying 2^+ states

The literature on the subject of pion elastic scattering and optical potentials is abundant.[19–22] The distorted-wave impulse approximation (DWIA) provides a model for describing inelastic pion scattering utilizing nuclear-structure information and the properties of the pion-nucleon interaction.[19] The simplest form of this model is the static DWIA in which effects due to intermediate delta propagation and interactions are ignored. There are different prescriptions for picking the interaction to be used and for including higher-order processes. The calculations presented here use the DWIA coordinate-space code DWPI[23] modified to allow explicit isospin separation in the Kisslinger form for the optical potential.[5] The nuclear density was taken as a Woods-Saxon distribution with the standard expansion of the radius in terms of the deformation parameter β_l or deformation length $\delta_l=\beta_l R_0$. Here one assumes different deformation parameters for the neutrons and protons. The neutron and proton geometry parameters were taken to be the same as that determined from electron scattering. The charge root-mean-square (rms) radius is 2.99 (3.06) fm for ^{24}Mg (^{26}Mg) and the diffuseness for each isotope is fixed at 0.52 fm in a two-parameter Fermi distribution.[24] Correcting the rms charge radius for the finite proton size (0.8 fm) constrains the nuclear radius parameter to be $R_0=2.75$ (2.88) fm. In the calculations discussed below, the neutron radius is set equal to that for the protons.

Calculations using the free π-nucleon t matrix yield poor fits to the elastic scattering data. Those which use the π-nucleon t matrix at a shifted incident pion energy of -25 to -30 MeV have been shown to give good fits to data for ^{12}C and ^{40}Ca at energies between 120 and 280 MeV.[25] Other authors have used the same prescription for isotopes of calcium[1] and for nuclei with $A\sim 52$.[26]

The calculations performed are compared with the experimental results obtained here for elastic scattering on ^{24}Mg and ^{26}Mg in Figs. 4–6. The π^+ (squares) and π^- (triangles) scattering data reported here on ^{24}Mg and ^{26}Mg at 150 MeV (Fig. 4) and on ^{26}Mg at 116, 180, and 292 MeV (Fig. 5), are all better described by the calculations which utilize the energy shift. Calculations with no energy shift are found to be inferior in all cases to those with a shift of -25 MeV. Similar calculations were also found to be in good agreement with the data of Ref. 17 on π^+ and π^- elastic scattering from ^{28}Si at 130, 180, and 226 MeV. Neutron and proton densities for the ^{28}Si calculations used had $R_0=2.95$ fm and $a=0.54$ fm, corresponding to the measured charge rms radius of 3.14 fm.

As in Ref. 5, inelastic DWIA calculations were simultaneously fitted to the π^+ and π^- data for the 2_1^+ state in ^{28}Si and 2_1^+ and 2_2^+ states of ^{24}Mg and ^{26}Mg by adjusting the proton and neutron deformation parameters β_{p2} and β_{n2}. The values of the deformation parameters and matrix elements M_p and M_n are given in Table I. In Table II, the matrix elements determined here are compared with results from other studies. The data of Ref. 17 on the excitation of the (1.78 MeV, 2^+) state in ^{28}Si were found to be explained by DWIA calculations utilizing $\beta_{p2}=0.58$ and $\beta_{n2}=0.56$. This corresponds to matrix elements M_p (M_n) equal to 21.7 (21.0) e fm^2 as compared with the electromagnetic value[27] of 18.2 ± 0.2 e fm^2. It is found that equal β_{p2} and β_{n2} cannot explain the data for $N=Z$ nuclei; this is also seen for the 2_1^+ and 2_2^+ states in ^{24}Mg (Fig. 4).

For $N=Z$ nuclei, deformations chosen such that $\beta_{p2}=\beta_{n2}$ result in predictions for differential cross sections ($d\sigma_{\pi^+}$ and $d\sigma_{\pi^-}$) at the first maximum that are sys-

tematically higher for π^- than π^+. This can be attributed to the Coulomb interaction, as calculations for π^0 scattering are found to be the median of the π^+ and π^- calculations. This difference is not seen in the data, where the ratios of $d\sigma_{\pi^-}/d\sigma_{\pi^+}$ for ^{28}Si (Ref. 17) are 0.96 (11), 0.92 (6), 0.96 (6), and 0.98 (4) for ^{24}Mg.[2] The difference also was not large for ^{12}C and ^{40}Ca.[20]

The phenomenon is illustrated in Fig. 6 in which the peak of the angular distribution for the 2^+ state in ^{24}Mg is given as a function of the incident pion energy. In the top half of the figure, calculations with equal β_{p2} and β_{n2} are seen to result in systematically greater π^- cross sections than π^+ cross sections. At 180 MeV this calculated ratio of π^- and π^+ peak cross sections is 1.14. The data reported are nearly equal, with a ratio of 0.96 ($\pm$0.03), and require β_{p2} (β_{n2})=0.82 (0.74) for the 2_1^+ and 0.20 (0.18) for the 2_2^+. In fact, at all angles and for all states in ^{24}Mg (except for the peak observed at 15.4 MeV), $d\sigma_{\pi^-} \sim d\sigma_{\pi^+}$. (The difference in the excitation of the peak at 15.4 for π^+ and π^- is evident in Fig. 2.) For the higher-lying states, the ratios of β_{pL}/β_{nL} are found to be consistent (1.1)–(1.2) with that for the 2_1^+. The results of the calculations found in the bottom of Fig. 6 imply that $d\sigma_{\pi^+}$ is larger than $d\sigma_{\pi^-}$ for energies greater than the (3,3) delta resonance and less at energies below 100 MeV. The matrix elements for the two 2^+ states are seen in Table II to be in agreement with values from electromag-

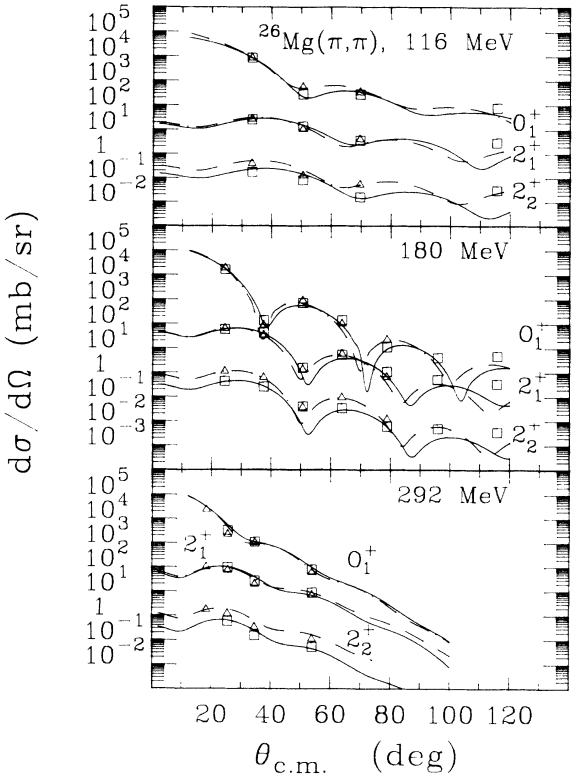

FIG. 5. Same as Fig. 4 for 116, 180, and 292 MeV π^+ and π^- scattering from ^{26}Mg.

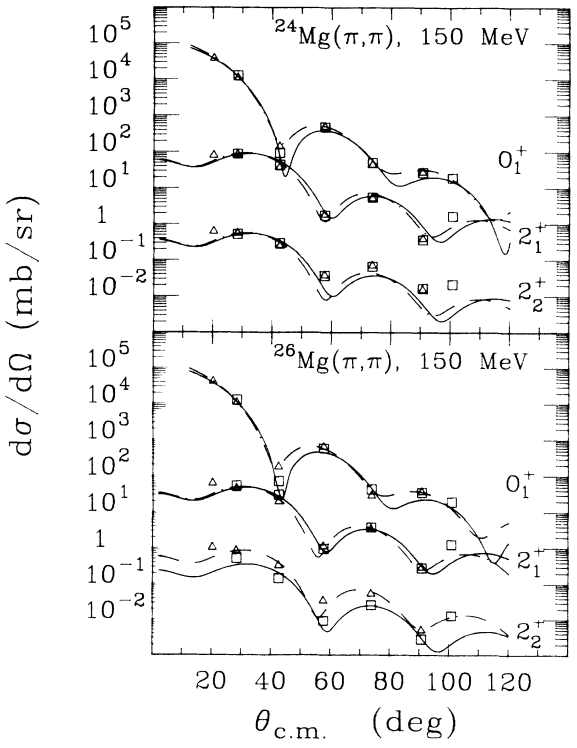

FIG. 4. Angular distributions of elastic and inelastic 2_1^+ and 2_2^+ states scattering of π^+ and π^- from ^{24}Mg and ^{26}Mg at 150 MeV. The π^+ (π^-) data are given as squares (triangles) while the calculations are given by solid (dot-dashed) lines.

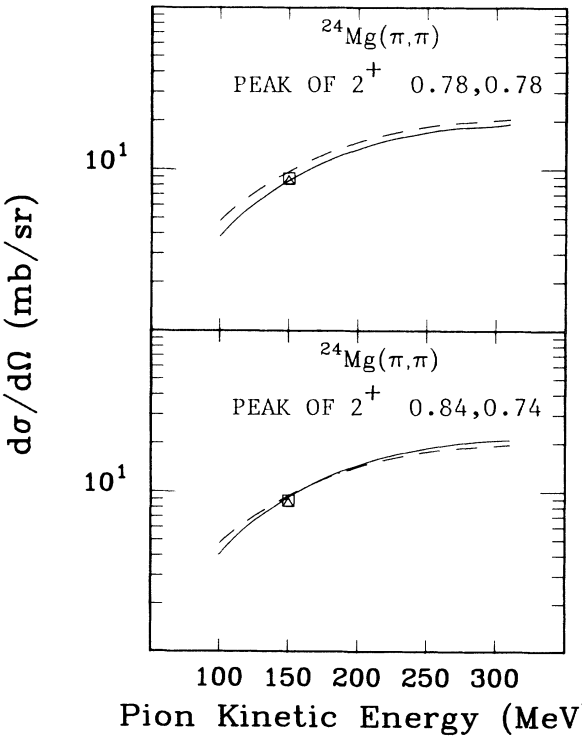

FIG. 6. Calculated value of the differential cross section at the first maximum in the angular distribution of pion exciting the 2_1^+ state in ^{24}Mg. In the top of the figure, $\beta_{p2}=\beta_{n2}=0.78$. In the bottom of the figure $\beta_{p2}=0.84$, $\beta_{n2}=0.74$.

netic studies, (p,p') and shell-model calculations (generally within 10%).

These calculations included the nuclear, Coulomb and Coulomb-nuclear interference terms in the Klein-Gordon equation. The effects of including the Coulomb-squared terms were found to be negligible. The effects of Coulomb excitation in pion inelastic scattering has also been found to be negligible. In previous work on inelastic scattering in strongly absorptive systems the value of $\beta_l R$ has been found to be constant as a function of energy and probe. Here one finds that agreement with the data for the 2_1^+ in ^{24}Mg can be obtained by reducing the neutron radius parameter from 2.75 to 2.50 fm and using $\beta_{p2}=\beta_{n2}=0.82$. This keeps the same ratio of $\beta_p R_p/\beta_n R_n$ and gives the same inelastic cross sections at the peak of the angular distributions. The effect on the elastic cross sections is mainly in the regions of the minima and maxima. The calculated π^+ elastic cross section increases by 24% at the first minimum and decreases by 5% at the first maximum, while the π^- elastic cross section decreases by 20% at the first minimum and decreases by 13% at the first maximum. Therefore, in this model the data can be explained either by a difference in β_p/β_n or in R_p/R_n. Here a difference in β_p/β_n will be utilized. Since equal β's and R's are preferred in $N=Z$ nuclei, this difference can be interpreted as a measure of the failure of the model. Here this will be assumed to be a source of error in the determination of the β_p/β_n differences in ^{26}Mg. This systematic error of 11% dominates the small statistical errors in the data.

Deformations of $\beta_{p2}(\beta_{n2})=0.56(0.49)$ for the 2_1^+ and 0.10 (0.25) for the 2_2^+ in ^{26}Mg result in the curves found in Figs. 4 and 5. The agreement with the data is generally good and the energy dependence of the first maxima is also well described. The structure of the angular distributions at 292 MeV is not as well explained. The values of matrix elements for exciting the (1.81 MeV, 2^+) state given in Table I are slightly larger than those of Ref. 5 with a slightly larger ratio of $M_n/M_p \sim 1.02$, compared with 0.92. Both results are larger than those of Refs. 3 and 4. In Ref. 4, the strength of the calculations are matched to the data, but the slope defined by the data is not reproduced by the calculations and that slope does not extend across the first maximum. In Table II one sees that the M_p for the 1.81 MeV state is in good agreement with the values from EM measurements and shell-model calculations, but is somewhat larger than that from (p,p'). M_n is in agreement with that implied from measurements[9] for the mirror nucleus ^{26}Si and is larger than that found in shell-model calculations. The ratio of M_n/M_p is in good agreement with that from electromagnetic studies,[9] 1.06 (6). The values of M_n, M_p for the (2.94, 2^+) state in ^{26}Mg are in good agreement with the shell model, but M_n is larger than the value for the mir-

TABLE I. Values of deformation parameters used in the DWIA analyses (discussed in the text) and the corresponding matrix elements, compared with previous measurements of pion inelastic scattering.

Excitation energy (MeV)	L	β_{pL}, β_{nL}	M_p, M_n (e fm^L)	Other (π,π')
		^{24}Mg		
1.36	2	0.82, 0.74	23.2, 20.9	$\beta_2=0.82$[a]
4.14	2	0.20, 0.18	5.8, 5.2	
5.93	4	0.36, 0.32	161, 143	$\beta_4=0.38$[a]
7.55	3	0.28, 0.24	30.9, 26.3	$\beta_3=0.35$[a]
8.33	3	0.37, 0.30	39.8, 33.0	
9.32	4	0.14, 0.12	61, 52	
9.97	5	0.27, 0.23	535, 456	
11.08	3	0.17, 0.14	18.6, 15.2	
13.96	3	0.13, 0.11	13.7, 12.3	
		^{26}Mg		
1.81	2	0.56, 0.49	17.0, 17.4	$M_p=16.5(10)$, $M_n=15.1(11)$[b] $\beta_p=0.655$, $\beta_n=0.459$[c]
2.92	2	0.10, 0.25	3.0, 8.8	
4.31	2	0.061, 0.054	1.9, 1.9	
	4	0.20, 0.15	102, 87	
4.90	4	0.19, 0.18	94, 104	
5.31	2	0.037, 0.098	1.1, 3.5	
5.44	4	0.10, 0.19	52, 112	
5.69	4	0.18, 0.074	91, 43	
6.86	3	0.21, 0.25	24.9, 34.4	
7.33	3	0.22, 0.22	26.3, 31.4	
7.79	3	0.20, 0.13	23.5, 18.3	
8.17	3	0.20, 0.25	24.4, 34.5	
10.30	4	0.17, 0.15	85, 88	

[a]Reference 2.
[b]Reference 5.
[c]Reference 4.

ror nucleus[9] so that the ratio obtained here is larger than the EM ratio.[12]

B. Natural parity states of spin 2, 3, 4, or 5

Data for higher-lying states have been analyzed in the same manner as those for the first two 2^+ states. For ^{24}Mg the ratio of β_{pL}/β_{nL} was allowed to differ but generally remained between 1.1–1.2. The results of the calculations for states in ^{24}Mg are shown in Fig. 7. The values of the deformation parameters are given in Table I and the derived matrix elements are given in Tables I and II. Generally, where comparison is possible, values of matrix elements obtained here are in agreement with those obtained from other work. The shell-model calculations, which employ *s-d* shell nucleons within the shell only and one value for the effective charge, are able to reproduce the general strength of M_p and M_n for the 2^+ and 4^+ states and correctly predict whether the ratio is less than or greater than 1.

As seen in the figure the fits to the first maximum in the angular distributions for the (5.93, 4^+) and 3^- states at 7.55, 8.33, 11.08, and 13.96 MeV are good. The collective model $L=4$ angular distribution for the (5.93, 4^+) state in ^{24}Mg and those for the 4^+ states in ^{26}Mg fail by a factor of 2 to explain the rise at the second maximum in the data. The fits to the 3^- states in Fig. 7 are better, but also fall too fast compared to the data for the 7.55, 11.08 and 13.96 MeV states. The data for the 8.33 MeV state is

TABLE II. Matrix elements (in $e\,\mathrm{fm}^L$) determined in this experiment compared with values from electromagnetic measurements (EM), 0.8 GeV proton inelastic scattering, and shell-model calculations (SM).

Energy	L	M_p, M_n (pion)	M_p (EM)	M (proton)[a]	M_p, M_n (SM)[b]
			^{24}Mg		
1.36	2	23, 21	21.3(8)[c]	19.9	18.6, 18.6
			20.4(6)[d]	(18.7)[CC]	
			21.8(10)[a]		
			20.5(7)[a]		
			20.5(6)[a]		
4.14	2	5.8, 5.2	5.2(3)[c]	4.8	−5.6, −5.6
5.93	4	160, 140	207.(14)[c]	203	169, 169
			205.(24)[d]		
7.55	3	31, 26	37.(3)[d]	32	
8.33	3	40, 33	45.(3)[d]	37	
9.32	4	61, 52	($L=2$)		($E=9.6$) 14.7
9.97	5	540, 460		690	
11.08	3	19, 15		15	
13.96	3	14, 12			
			^{26}Mg		
1.81	2	17.0, 17.4	16.5(6)[e]	15.1	17.3, 13.9
			17.2(8)[a]	(15.2)[CC]	
			[17.8(4), 18.8(9)][f]		
2.92	2	3.0, 8.8	2.7[e]	4.9	3.0, 9.6
			[3.0(2), 6.0(7)][f]		
4.31	2	1.9, 1.9	1.6[e]	2.2	−0.8, −2.2
			[2.7(4), 3.5(7)][f]		
	4	102, 89		66	−88, −69
4.90	4	94, 104	184[e]	109	108, 140
5.31	2	1.1, 3.5	1.9[e]	2.9	2.5, 2.8
5.44	4	52, 112	68[e]	61	10, −68
5.69	4	91, 43	130[e]	63	−85, −48
6.86	3	25, 34	27[e]	24	
7.33	3	26, 31			
7.79	3	24, 18		19	
8.17	3	24, 34		24	
10.30	4	85, 88	(10.7 MeV)98[e]	74	(small)

[a](p,p') at 0.8 GeV of Refs. 10 and 11. From moments of deformed imaginary potential of a DWBA analysis, except where noted. CC=coupled channels with rotational model.
[b]Shell-model results of Ref. 12.
[c]Reference 6.
[d]Reference 7.
[e]Reference 8.
[f]Reference 9.

below the calculation at the second maximum. The fits to the 9.32 and 9.97 MeV states are poor.

Results for states in ^{26}Mg are found in Figs. 8–17. As in Ref. 11, an incoherent sum of calculations for an $L=2$ and $L=4$ excitation for the (4.3, 2^+ and 4^+) doublet is found in Fig. 8 to explain the forward-angle data at 116, 150, and 180 MeV, but fails to describe the data at 292 MeV.

The data in the region of the first maximum in the angular distribution for the (4.9, 4^+) state in ^{26}Mg at 116, 150, and 180 MeV are well explained by the $L=4$ collective form factor, but the data in the region of the second maximum are consistently higher than the calculations, and the data at 292 MeV are not well described (Fig. 9). The M_p, M_n values are consistent with the (p,p') values and the shell-model predictions. The EM measurement is nearly a factor of 2 higher and is equal to the sum of values for the 4.3 and 4.9 MeV states.

The values of the π^- and π^+ cross sections at the first maximum in the angular distributions give M_p, M_n for the (5.31, 2^+) state in (Fig. 10) consistent with other measurements and which suggest that the state is largely given by neutron excitations with $M_n/M_p > 3$. The results for the (5.44, 4^+) and the (5.69, 4^+) (Figs. 11 and 12) confirm the shell-model predictions that M_n/M_p is $\gg 1$ for the 5.44 MeV state and $\ll 1$ for the 5.69 MeV state. The EM value of M_p for the 5.69 MeV state is higher than the other determinations. Data for four 3^- states found in Figs. 13–16 are well explained by the collective-model calculations. The strengths of the four states are comparable and agree with the (p,p') results and the one (e,e') result.

The data for the 10.3 MeV state (Fig. 17) are well explained at each energy. The M_p, M_n values are nearly equal and are slightly larger than the (p,p') result. The (e,e') result for a state given to be 10.7 MeV is also consistent with this value. The shell model predicts only 4^+ states with much smaller matrix elements at this excitation energy.

C. Monopole transitions

Data and calculations employing monopole form factors are found in Figs. 18 and 19 for the (6.44, 0^+) state in ^{24}Mg and the (3.59, 0^+) state in ^{26}Mg. To include monopole transitions in the collective model description of ^{24,26}Mg, a model must be constructed which satisfies the requirement of orthogonality of the initial and final

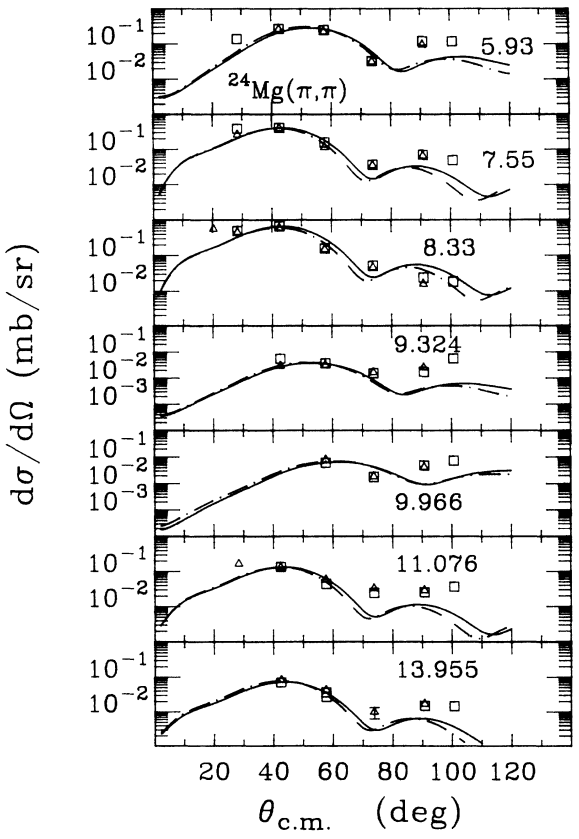

FIG. 7. Pion inelastic scattering exciting the (5.93, 4^+), (7.55, 3^-), (8.33, 3^-), (9.324), (9.966), (11.076, 3^-), and (13.955, 3^-) states in ^{24}Mg. The π^+ (π^-) data are given as squares (triangles) while the calculations are given by the solid (dot-dashed) lines. The deformation parameters are given in Table I.

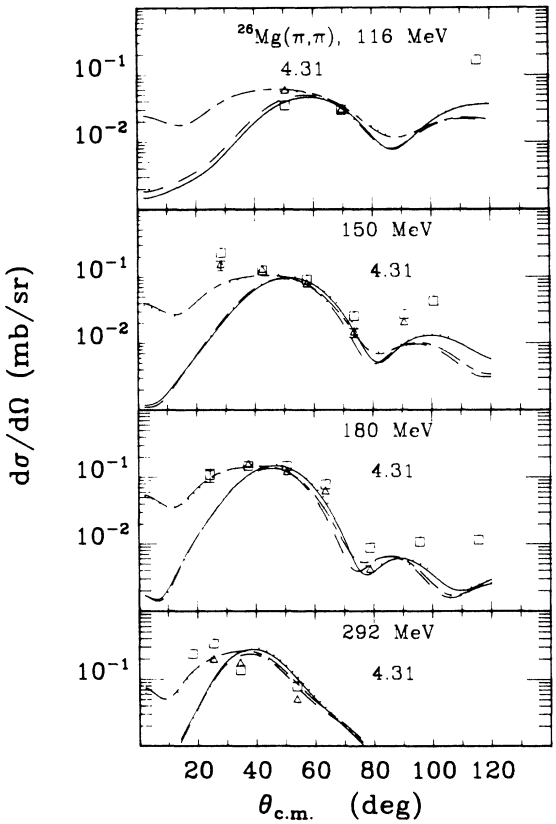

FIG. 8. Same as Fig. 7 for the (4.31, 2^+ and 4^+) states in ^{26}Mg. The solid (dot-dashed) lines correspond to π^+ (π^-) excitation of the 4^+ state while the dotted (long-dashed) lines are the incoherent sum.

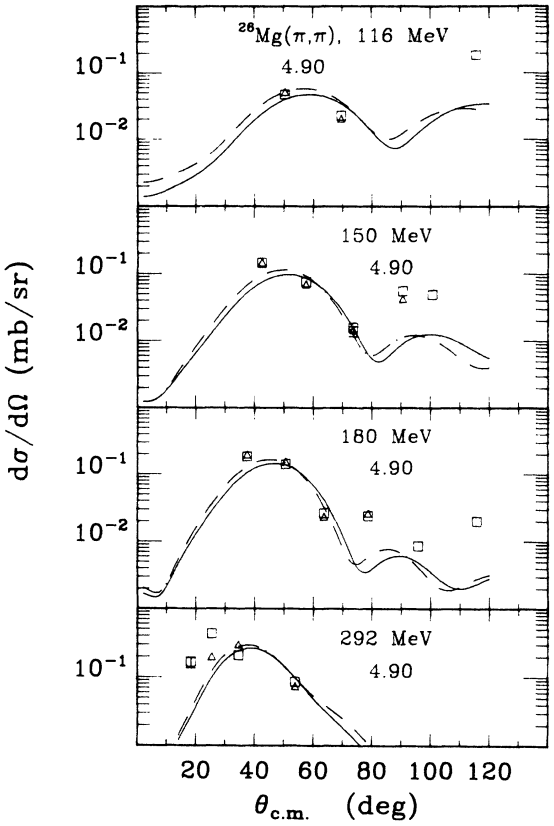

FIG. 9. Same as Fig. 8 for the (4.90, 4^+) state in ^{26}Mg.

states. This cannot be done with a simple positive-definite-derivative transition density, as was the case for transitions with $l > 1$. In collective models, monopole transitions involve radial oscillations. Although the low compressibility of nuclear matter makes such models

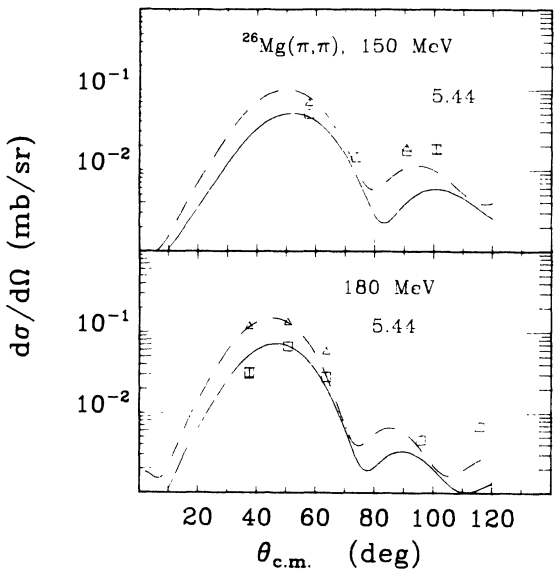

FIG. 11. Same as Fig. 8 for the (5.44, 4^+) state in ^{26}Mg.

most appropriate for describing monopole giant resonances, low-lying 0^+ states can be included in the formalism by adjusting the parameters to electron scattering data.

In the Tassie model, to lowest order, conservation of nucleon number and the orthogonality of the wave functions for the initial and final states requires a monopole transition density given by

$$\delta\rho_0(r) = -\alpha_0 \left[3\rho(r) + r\frac{d\rho(r)}{dr} \right]$$

where α_0 is the monopole transition strength parameter

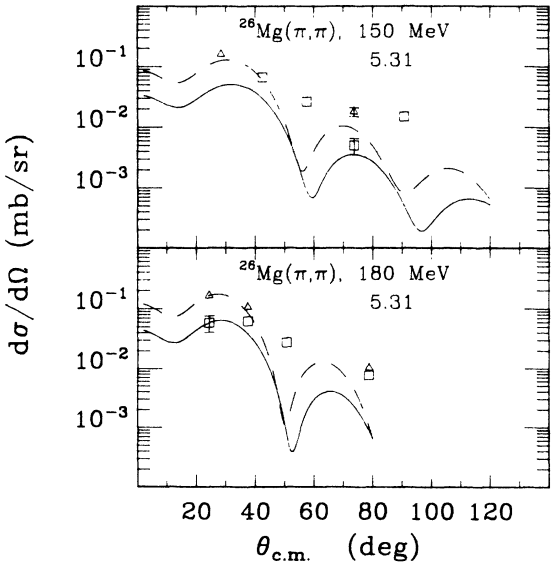

FIG. 10. Same as Fig. 8 for the (5.31, 2^+) state in ^{26}Mg.

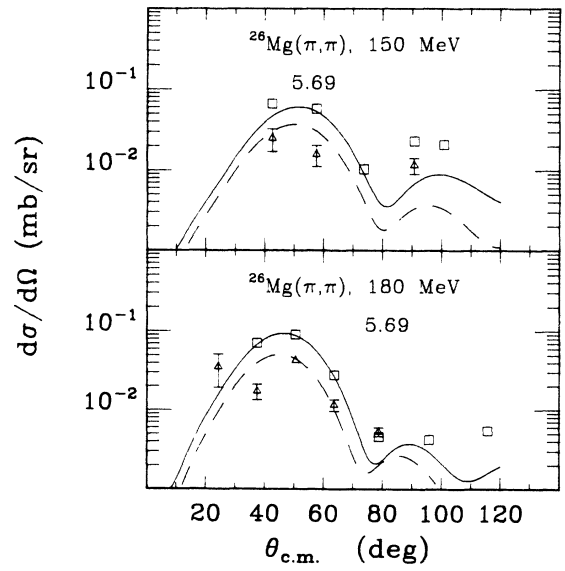

FIG. 12. Same as Fig. 8 for the (5.69, 4^+) state in ^{26}Mg.

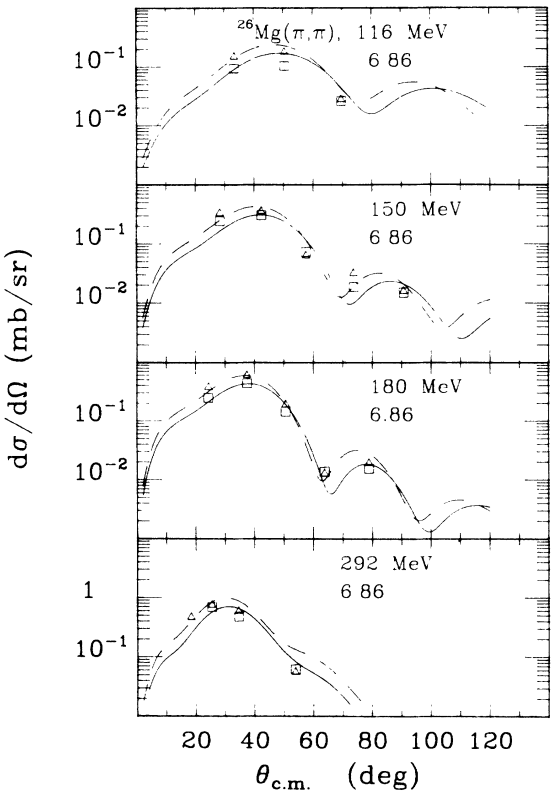

FIG. 13. Same as Fig. 8 for the (6.86, 3$^-$) state in ^{26}Mg.

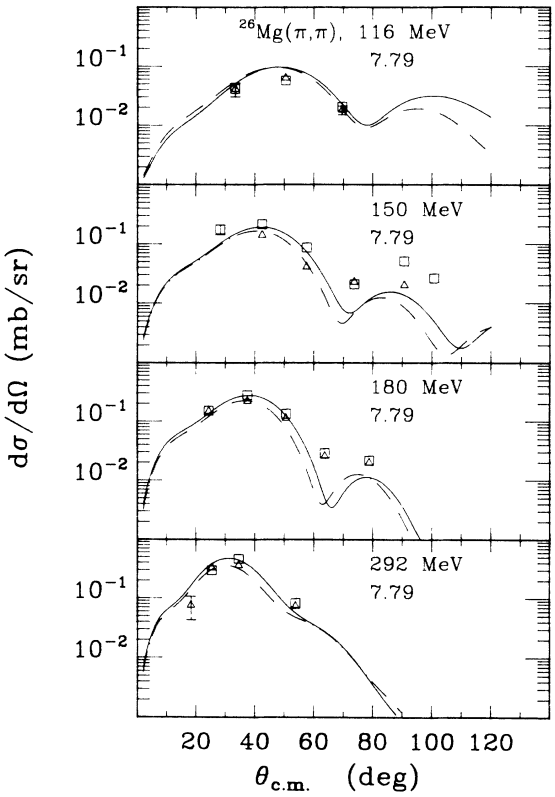

FIG. 15. Same as Fig. 8 for the (7.79, 3$^-$) state in ^{26}Mg.

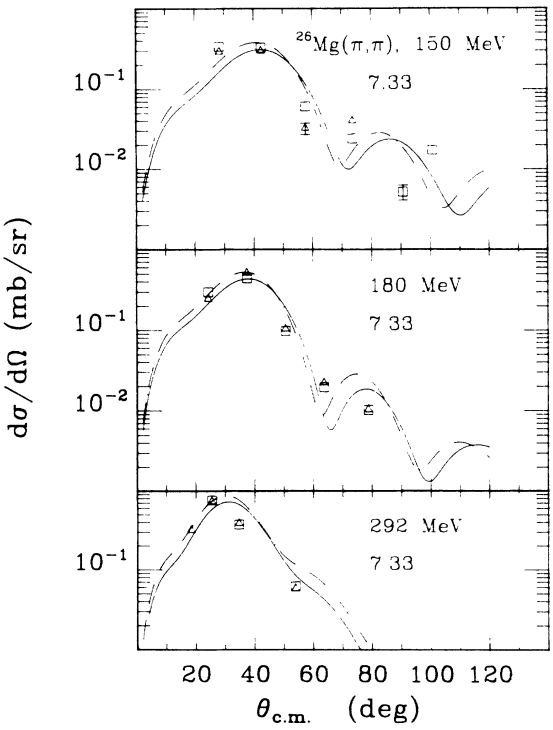

FIG. 14. Same as Fig. 8 for the (7.33, 3$^-$) state in ^{26}Mg.

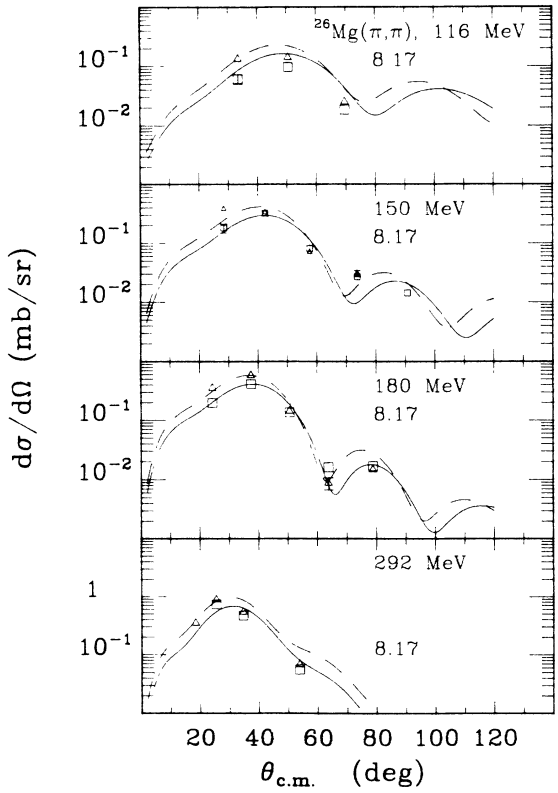

FIG. 16. Same as Fig. 8 for the (8.17, 3$^-$) state in ^{26}Mg.

and $\rho(r)$ is the nuclear density. Choosing the density to have a harmonic oscillator form, the transition density can be written as

$$\delta\rho_0(r)=(b\sqrt{\pi})^{-3}[A+B(r/b)^2+C(r/b)^4]e^{-(r/b)^2},$$

where b is the oscillator length parameter and A, B, and C are functions of the monopole matrix element C_0 and the transition radius R_{tr}.

The monopole form factors for the 0_2^+ states in both ^{24}Mg (Refs. 7 and 28) and ^{26}Mg (Ref. 8) have been measured for momentum transfers up to ~ 1 fm^{-1}. Fitting the above transition density form to these data gives $C_0=6.66$ fm, $R_{tr}=6.06$ fm, and $b=2.71$ fm for ^{24}Mg and $C_0=4.23$ fm, $R_{tr}=6.17$ fm, and $b=2.76$ fm for ^{26}Mg. From these values the transition density parameters for ^{24}Mg are $A=-7.55\times10^{-2}$, $B=5.036\times10^{-2}$, $C=4.257\times10^{-6}$ and for ^{26}Mg, $A=-4.633\times10^{-2}$, $B=3.093\times10^{-2}$, and $C=-1.547\times10^{-5}$.

Previous investigations of pion-induced monopole transitions in ^{12}C (Refs. 29–31) and ^{28}Si (Refs. 32 and 33) found that the distorted-wave formalism is inadequate to account for the angle or energy dependence of the data. By including a two-step contribution through the 2_1^+ state the agreement with the data is improved. The need for this more detailed treatment of the reaction dynamics is most dramatic at energies below 100 MeV where the pion mean free path is longer and the momentum transfer is smaller. At small momentum transfer, the direct transition arises primarily from the distortions in the incom-

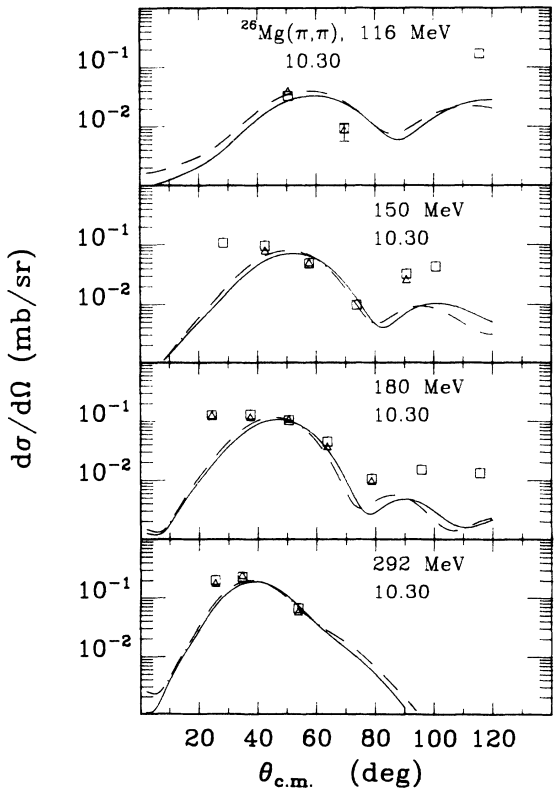

FIG. 17. Same as Fig. 8 for the (10.3, 4$^-$) state in ^{26}Mg.

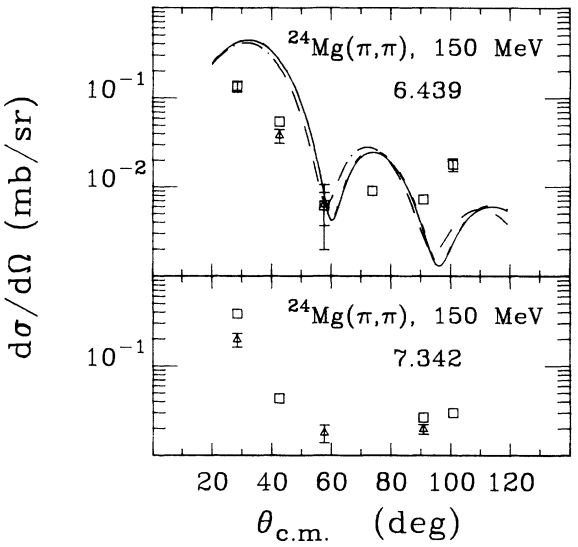

FIG. 18. Same as Fig. 8 for the (6.439, 0$^+$) and (7.342) states in ^{24}Mg. The curves result from coupled-channel calculations as discussed in the text. The dashed curve results from a calculation with only direct excitation.

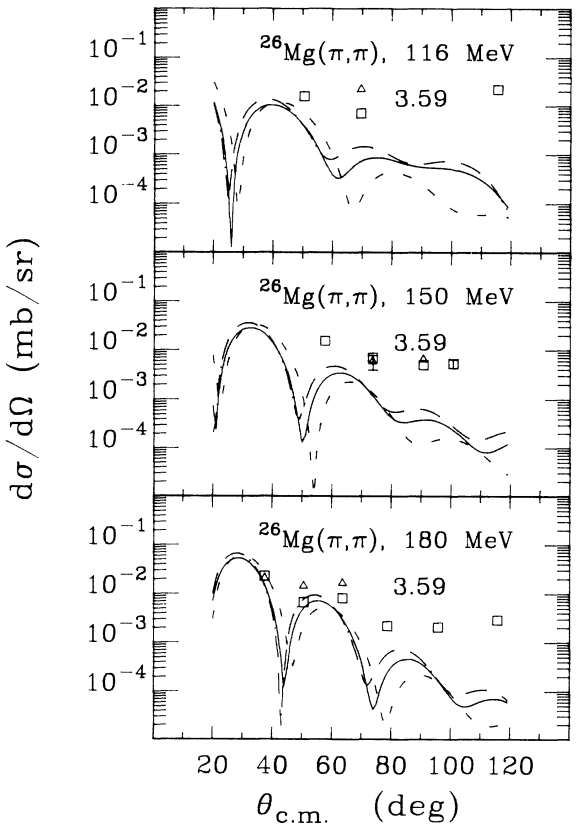

FIG. 19. Same as Fig. 8 for the (3.59, 0$^+$) state in ^{26}Mg. The curves result from coupled-channel calculations as discussed in the text. The dashed curves results from calculations with only direct excitation.

ing and outgoing waves, producing a small cross section. At low energies the interference between the one- and two-step processes can have a large effect. While this effect is confined to angles less than about 25° at resonance energies, one still finds significant differences in the location and depth of diffraction minima at all angles.

The calculations for the 0_2^+ states in ^{24}Mg and ^{26}Mg have been done in a coupled channels (CC) framework using the code CHOPIN.[34] The 0_2^+ state is coupled, in the CC calculation, to the ground state, and to the 2_1^+ state with a strength that is derived from the β_2 that couples the 0_1^+-2_1^+ states by the ratio of the strengths of γ-ray transitions in these isotopes.[35]

Data were obtained for the 0_2^+, 6.44 MeV state in ^{24}Mg only at 150 MeV and are compared with the CC calculation in Fig. 18. The data for this transition are not reproduced by the calculation. Figure 19 shows the data for the 0_2^+, 3.59 MeV state in ^{26}Mg at 116, 150, and 180 MeV. At the higher energies where the data are more complete, the measured angular distributions appear to be relatively flat while the calculated cross sections exhibit deep minima. This discrepancy may be due in part to the uncertainty in the monopole form factor determined from electron scattering. The electron scattering data extend only to about 1 fm^{-1} which corresponds to ~40° at these energies. Thus, the calculations presented here depend essentially on the form of the transition density to provide a reasonable extrapolation to higher momentum transfer. However, the more complete results for ^{12}C at 162 MeV (Ref. 30) also show a similar discrepancy between data and calculation at momentum transfers where the ^{12}C monopole form factor is well determined.

A more likely source of error is the current treatment of the nuclear structure. In all calculations presented here, the nucleus is implicitly treated as vibrational. The higher-order effects which differentiate between the rotational and vibrational models are absent. The effect of the coupled channels is demonstrated by the dashed line in the figures, which results from a single-step excitation of the 0_2^+ states from π^+ scattering. This is to be compared with the solid curve in the figures. The coupled-channel effects for the 0_2^+ state in ^{24}Mg are very small and the failure of the model is difficult to repair with a more complete calculation. The effects for ^{26}Mg are larger and the results may be improved by an improved model.

IV. SUMMARY AND CONCLUSION

Measurements of angular distributions of positive and negative pions exciting approximately 40 states in ^{24}Mg and ^{26}Mg have been reported. The distorted-wave impulse approximation with a Kisslinger form for the optical potential and a prescription of evaluating the π-nucleon t matrix at a shifted energy of -25 MeV was found to explain π^+ and π^- elastic scattering data from ^{24,26}Mg and ^{28}Si in the energy range spanned by these data. Inelastic distorted-wave impulse approximation calculations employing collective-model deformation parameters were simultaneously fitted to the π^+ and π^- data for each state. The deformation parameters and matrix elements M_p and M_n in most cases compare favorably with results from other studies. The published shell-model calculations which employ *s-d* shell nucleons only and one value for the effective charges are found to reproduce the general strength of M_p and M_n for the 2^+ and 4^+ states observed here, and correctly predict whether the ratios of the matrix elements are less than or greater than 1. The data for ^{24}Mg and that from other studies for ^{12}C, ^{28}Si, and ^{40}Ca show that $d\sigma_{\pi^+}$ is approximately equal to $d\sigma_{\pi^-}$ at the first maximum in the inelastic angular distributions. This forces β_{pL} to be greater than β_{nL} and M_n/M_p to be less than unity. Here, this has been interpreted as a measure of the failure of the model which causes a systematic error of -11% in the ratio of M_n/M_p for states in ^{26}Mg. The monopole transition data are reproduced only in general magnitude by the coupled-channels calculations presented here. To adequately describe these data a more detailed account of the nuclear structure is required. Angular distributions of pions exciting known and candidate unnatural-parity 6^- states which are not presented here will form the subject of another work.

The research reported here is supported in part by the U.S. National Science Foundation, the U.S. Department of Energy, and the Robert A. Welch Foundation.

*Present address: Oregon Institute of Technology, Klamath Falls, Oregon 97601.

†Present address: Fermi National Accelerator Laboratory, Batavia, Illinois 60510.

‡Present address: Lawrence Berkeley Laboratory, Berkeley, California 94720.

§Present address: Argonne National Laboratory, Argonne, Illinois 60439.

[1]K. B. Boyer *et al.*, Phys. Rev. C **29**, 182 (1984).

[2]C.A. Wiedner *et al.*, Phys. Lett. **78B**, 26 (1978).

[3]C. A. Wiedner *et al.*, Phys. Lett. **97B**, 37 (1980).

[4]R. Tacik *et al.*, Phys. Rev. Lett. **52**, 1276 (1984).

[5]C. L. Morris *et al.*, Phys. Rev. C **35**, 1388 (1987).

[6]H. Zarek *et al.*, Phys. Lett. **80B**, 26 (1978).

[7]A. Johnson and T. E. Drake, J. Phys. A **7**, 898 (1974).

[8]E. W. Lees *et al.*, J. Phys. A **7**, 936 (1974).

[9]T. K. Alexander *et al.*, Phys. Lett. **113B**, 132 (1982).

[10]G. S. Blanpied *et al.*, Phys. Rev. C **25**, 422 (1982).

[11]G. S. Blanpied *et al.*, Phys. Rev. C **37**, 1987 (1988).

[12]B. A. Brown, R. Radhi, and B. H. Wildenthal, Phys. Rep. **101**, 314 (1983); B. H. Wildenthal, B. A. Brown, and I. Sick, Phys. Rev. C **32**, 2185 (1985).

[13]H. A. Theissen and S. Sobottka, Los Alamos National Laboratory Report No. LA-4534MS, 1970.

[14]S. J. Seestrom-Morris, Ph.D. thesis, University of Minnesota, 1981; Los Alamos National Laboratory Report No. LA8916-

T, 1981.
[15]R. A. Arndt and L. D. Roper, SAID-Scattering Analysis Interactive Dial In. Based on data file PN83-8 ofJune 2, 1983.
[16]L. E. Smith, computer program LOAF (unpublished).
[17]B. M. Preedom *et al.*, Nucl. Phys. **A326**, 385 (1979).
[18]See AIP Document No. PAPS PRVCA-41-1625-41 for 41 pages of numerical data for scattering of positive and negative pions from ^{24}Mg and ^{26}Mg. Order by PAPS number and journal reference from American Institute of Physics, Auxiliary Publication Service, 335 East 45th Street, New York, NY 10017. The prices are $1.50 for microfiche and $5 for photocopies. Airmail additional. Make checks payable to the American Institute of Physics.
[19]L. S. Kisslinger, Phys. Rev. **98**, 761 (1955).
[20]C. L. Morris, Phys. Rev. C **24**, 231 (1981).
[21]E. Oset and D. Strottman, Nucl. Phys. **A377**, 297 (1982).
[22]M.Gmitro, J. Kvasil, and R. Mach, Phys. Lett. **113B**, 205 (1982).
[23]R. A. Eisenstein and G. A. Miller, Comput. Phys. Commun. **11**, 95 (1976).
[24]C. W. DeJager, H. DeVries, and C. DeVries, At. Data Nucl. Data Tables **14**, 479 (1974).
[25]W. B. Cottingame and D. B. Holtkamp, Phys. Rev. Lett. **45**, 1828 (1980).
[26]D. S. Oakley *et al.*, Phys. Rev. C **35**, 1392 (1987).
[27]G. C. Ball *et al.*, Nucl. Phys. **A349**, 271 (1980).
[28]Otto Titze, Z. Phys. **220**, 66 (1969).
[29]D. A. Sparrow and W. J. Gerace, Phys. Rev. Lett. **41**, 1101 (1978).
[30]C. L. Morris *et al.*, Phys. Rev. C **30**, 662 (1984).
[31]C. S. Whisnant, Phys. Rev. C **40**, 1741 (1989).
[32]D. A. Sparrow and W. J. Gerace, Phys. Rev. C **29**, 949 (1984).
[33]C. S. Whisnant *et al.*, Phys. Rev. C **39**, 1935 (1989).
[34]E. Rost (unpublished).
[35]P. M. Endt, At. Data Nucl. Data Tables **23**, 3 (1979).